

1 **Skillful Multiyear Sea Surface Temperature Predictability in CMIP6 Models and**
2 **Historical Observations**

3
4
5 **Frances V. Davenport^{1,2}, Elizabeth A. Barnes², and Emily M. Gordon^{2,3}**

6
7 ¹Department of Civil and Environmental Engineering, Colorado State University, Fort Collins,
8 CO.

9 ²Department of Atmospheric Science, Colorado State University, Fort Collins, CO.

10 ³Department of Earth System Science, Stanford University, Stanford, CA.

11
12
13 Corresponding author: Frances Davenport (f.davenport@colostate.edu)
14
15

16 **Key Points**

- 17 • Neural networks can learn predictable signals of internal sea surface temperature variability
18 at 1-3, 1-5, and 3-7 year lead times
- 19 • Neural networks trained on climate model output can skillfully predict sea surface
20 temperature variability in historical observations
- 21 • Neural network skill in predicting observed sea surface temperature variability depends on
22 the climate model used for training

24 **Abstract**

25 We use neural networks and large climate model ensembles to explore predictability of
26 internal variability in sea surface temperature anomalies on interannual (1-3 year) and decadal
27 (1-5 and 3-7 year) timescales. We find that neural networks can skillfully predict SST anomalies
28 at these lead times, especially in the North Atlantic, North Pacific, Tropical Pacific, Tropical
29 Atlantic and Southern Ocean. The spatial patterns of SST predictability vary across the nine
30 climate models studied. The neural networks identify “windows of opportunity” where future
31 SST anomalies can be predicted with more certainty. Neural networks trained on climate models
32 also make skillful SST predictions in historical observations, although the skill varies depending
33 on which climate model the network was trained. Our results highlight that neural networks can
34 identify predictable internal variability within existing climate datasets and show important
35 differences in how well patterns of SST predictability in climate models translate to the real
36 world.

37 **Plain Language Summary**

38 We train neural networks (a machine learning model) to predict sea surface temperature
39 between 3 and 7 years in the future. The neural networks are trained using data from existing
40 climate model simulations. The regions where neural networks make the most accurate
41 predictions depend on which climate model is used for training. The neural networks also make
42 accurate predictions using historical observations, which means some of the patterns learned
43 from the climate models also apply to the real climate system. However, there are unique
44 differences between prediction accuracy in climate models and observations, which suggests
45 directions for future research.

46 **1 Introduction**

47 Skillful predictions of regional climate variability on multiyear to decadal timescales
48 would provide valuable information for near-term societal decision making and adaptation
49 (Findell et al., 2023; Kushnir et al., 2019). While this goal remains a significant challenge, a
50 number of studies have shown potential for predicting patterns of internal climate variability,
51 particularly those related to large-scale ocean variability. For example, some patterns of ocean
52 variability thought to have predictable components on three- to-ten year timeframes include the
53 El-Nino Southern Oscillation (ENSO), Atlantic Multidecadal Variability (AMV), and the Pacific
54 Decadal Oscillation (PDO)(Cassou et al., 2018; Meehl et al., 2009; Van Oldenborgh et al.,
55 2012). These oceanic patterns can also lead to predictability of important processes over land,
56 including rainfall over the Sahel (Martin & Thorncroft, 2014), North American precipitation
57 (Enfield et al., 2001), Atlantic Hurricane frequency (Smith et al., 2010), late winter precipitation
58 over Western Europe (Simpson et al., 2019), and North American and European summer
59 temperatures (Sutton & Hodson, 2005).

60 Many recent insights into multiyear climate prediction come from initialized decadal
61 hindcast experiments, where model simulations are initialized to match historical observations as
62 closely as possible, and then run for up to a decade (e.g. Delgado-Torres et al., 2022; Meehl et
63 al., 2021; Yeager et al., 2018). The hindcast simulation can then be verified against what actually
64 occurs in the observations. Higher prediction skill is achieved when more ensemble members
65 are included in a hindcast experiment, with often at least 10, and sometimes as many as 40,

66 ensemble members used (Meehl et al., 2021). The computational expense associated with these
67 experiments thus poses a considerable challenge for decadal prediction. Initialized simulations
68 are also subject to model drift, which occurs when a simulation that has been initialized to match
69 observations drifts towards its own model climatology. How exactly initialized forecasts should
70 be corrected to account for this drift presents an additional challenge for decadal prediction
71 (Meehl et al., 2022; Risbey et al., 2021).

72 More recently, data-driven or machine learning (ML) based approaches have been used
73 to explore multiyear climate predictability (e.g. Gordon et al., 2021; Qin et al., 2022; Toms et al.,
74 2021). In these studies, a statistical or ML model is trained to predict a climate variable or
75 pattern of interest using existing climate datasets. Because of the need for large amounts of
76 training data, many (although not all) prior studies have focused on multiyear predictability
77 within large climate model simulations. For example, Toms et al. (2021) and Gordon et al.
78 (2021) both use 1,200 years or more from the pre-industrial control run of the Community Earth
79 System Model Version 2 (CESM2) to analyze predictability of land surface temperatures and the
80 PDO, respectively.

81 A clear benefit of ML-based approaches is the potential to learn about predictability of
82 the climate system from existing coupled atmosphere-ocean general circulation model (GCM)
83 simulations, reducing the need for additional initialized simulations. However, as with any
84 approach that relies on GCM simulations, the trained ML models are subject to any biases
85 present in the underlying simulations. A few studies have explored whether ML models trained
86 on GCMs can make accurate predictions in observations. For example, Labe and Barnes (2022)
87 show that a neural network trained on CESM2 can predict observed global warming slowdowns.
88 Ham et al. (2019) show skillful predictions of observed ENSO variability with up to 17 month
89 lead times using a neural network trained on simulations from different GCMs. These studies
90 show potential for using ML models to predict observed climate variability, but whether or not
91 multiyear predictability in climate models reflects predictability of the real climate system more
92 broadly is still an open question.

93 Here, we analyze the predictability of sea surface temperature (SST) using neural
94 networks and historical simulations from the Coupled Model Intercomparison Project Phase 6
95 (CMIP6) archive (Eyring et al., 2016). We focus specifically on predicting internal variability of
96 SSTs at interannual (1-3 year) and decadal (1-5 and 3-7 year) timescales, and apply our analysis
97 globally. In order to have sufficient training data, we analyze GCMs that have at least 30
98 historical simulations. After evaluating SST predictability within each GCM, we analyze
99 whether the information learned by the neural networks can lead to accurate SST predictions
100 when tested on historical observations. Our goal is (i) to provide an overview and comparison of
101 patterns of SST predictability across different GCMs in the CMIP6 archive and (ii) to identify
102 regions where the SST predictability learned from GCMs provides the most skillful predictions
103 of the real ocean.

104 **2 Materials and Methods**

105 *2.1 CMIP6 data*

106 We analyze monthly SST data from nine GCMs that have at least 30 historical
107 simulations in the CMIP6 archive: *ACCESS-ESM1-5* (Ziehn et al., 2020), *CanESM5* (Swart et
108 al., 2019), *CNRM-CM6-1* (Voldoire et al., 2019), *GISS-E2-1-G* (Kelley et al., 2020), *IPSL-*

109 *CM6A-LR* (Boucher et al., 2020), *MIROC-ES2L* (Hajima et al., 2020), *MIROC6* (Tatebe et al.,
 110 2019), *MPI-ESM1-2-LR* (Mauritsen et al., 2019), and *NorCPMI* (Bethke et al., 2021). The
 111 historical simulations span 1850-2014, giving a total of 4,950 model-years for each GCM.

112 Before neural network training, we preprocess the data for each GCM. First, we regrid all
 113 climate model output to a common $5^\circ \times 5^\circ$ latitude-longitude grid. We analyze latitudes between
 114 65S to 65N. We calculate 12-month, 36-month and 60-month average SSTs at each grid point.
 115 From each time series (12-month, 36-month and 60-month averages), we subtract the ensemble-
 116 mean for each year at each grid point. By removing the ensemble mean response to external
 117 forcing, we focus our analysis on learning predictable components of internal climate variability.
 118 Once the ensemble mean is removed, we calculate the mean and standard deviation of SSTs at
 119 each grid point and use these to calculate standardized SST anomalies at each grid point at each
 120 timestep. Lastly, we calculate tercile limits at each grid point that are used to classify each SST
 121 anomaly as negative (bottom third), neutral (middle third), and positive (top third). The tercile
 122 limits are calculated separately for each simulation because some simulations are consistently
 123 cooler or warmer than the ensemble mean over the historical simulation period. Calculating the
 124 terciles separately creates a balanced number of negative, neutral, and positive anomalies within
 125 each simulation.

2.2 Neural network architecture and training

127 We train convolutional neural networks (CNNs) to predict SST anomalies using the
 128 GCM output (Figure 1). The CNN takes four global maps of prior SSTs as input. These maps
 129 correspond to SSTs averaged over 0-1 years, 1-2 years, 2-3 years, and 3-8 years prior. While
 130 variables such as ocean heat content may also be useful predictors, we only use sea surface
 131 temperature so that we can test the CNN using globally available sea surface temperature
 132 observations (see Section 2.4). For each set of input maps, the CNN predicts the SST anomaly at
 133 a given location (one grid cell) at a given time in the future. Each prediction is the relative
 134 likelihood of three categories: positive SST anomaly (the top tercile of historical anomalies),
 135 neutral anomaly (middle tercile), or negative anomaly (bottom tercile).

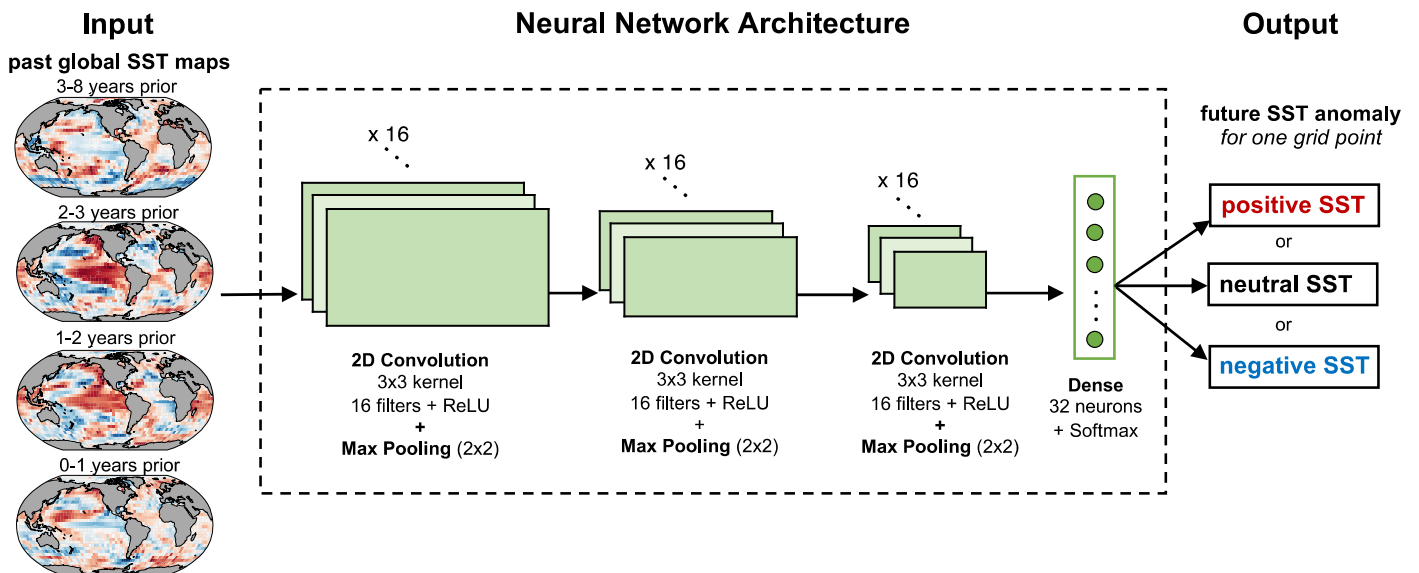


Figure 1. Overview of CNN architecture

136 We make SST predictions for three future time periods: years 1-3 (i.e. 36 month SST
137 anomalies starting from the prediction date), years 1-5 (i.e. 60 month SST anomalies starting
138 from the prediction date), and years 3-7 (i.e. 60 month SST anomalies starting 2 years after the
139 prediction date). We train separate CNNs for each ocean grid cell, lead time, and GCM (over
140 30,000 CNNs in total).

141 We split the 30 historical simulations from each GCM into a training set of 22
142 simulations, a validation set of three simulations, and a test set of five simulations (*Supporting*
143 *Information*, Table S1). We use hyperparameter tuning to select the CNN architecture shown in
144 Fig. 1. Details of the hyperparameter tuning and CNN training are included in the *Supporting*
145 *Information*.

146 *2.3 Neural network accuracy and windows of opportunity*

147 After training, we evaluate CNN performance on the testing data (five simulations per
148 GCM). First, we calculate prediction accuracy across all testing data. We also examine whether
149 the CNNs identify “*windows of opportunity*”, or states of internal variability that are more
150 predictable than others. We use the method from Mayer and Barnes (2021) and Gordon et al.
151 (2023) to calculate accuracy for subsets of predictions with the highest “confidence”, i.e. the
152 samples where the CNN predicts a higher relative likelihood of one class versus the others.
153 Higher prediction accuracy among more confident predictions indicates that the CNN has
154 successfully identified windows of opportunity where predictions are more likely to be skillful.
155 We calculate accuracy for the 40% and 20% most confident predictions within each testing
156 simulation, and then average across the five testing simulations for each GCM.

157 We compare the neural network accuracy to a persistence model, which assumes that the
158 future SST anomaly remains unchanged. For example, the SST anomaly prediction for year 1-5
159 is the same as the SST anomaly for the most recent 5 year period. Because there is no confidence
160 associated with these predictions, we only calculate overall accuracy (not windows of
161 opportunity).

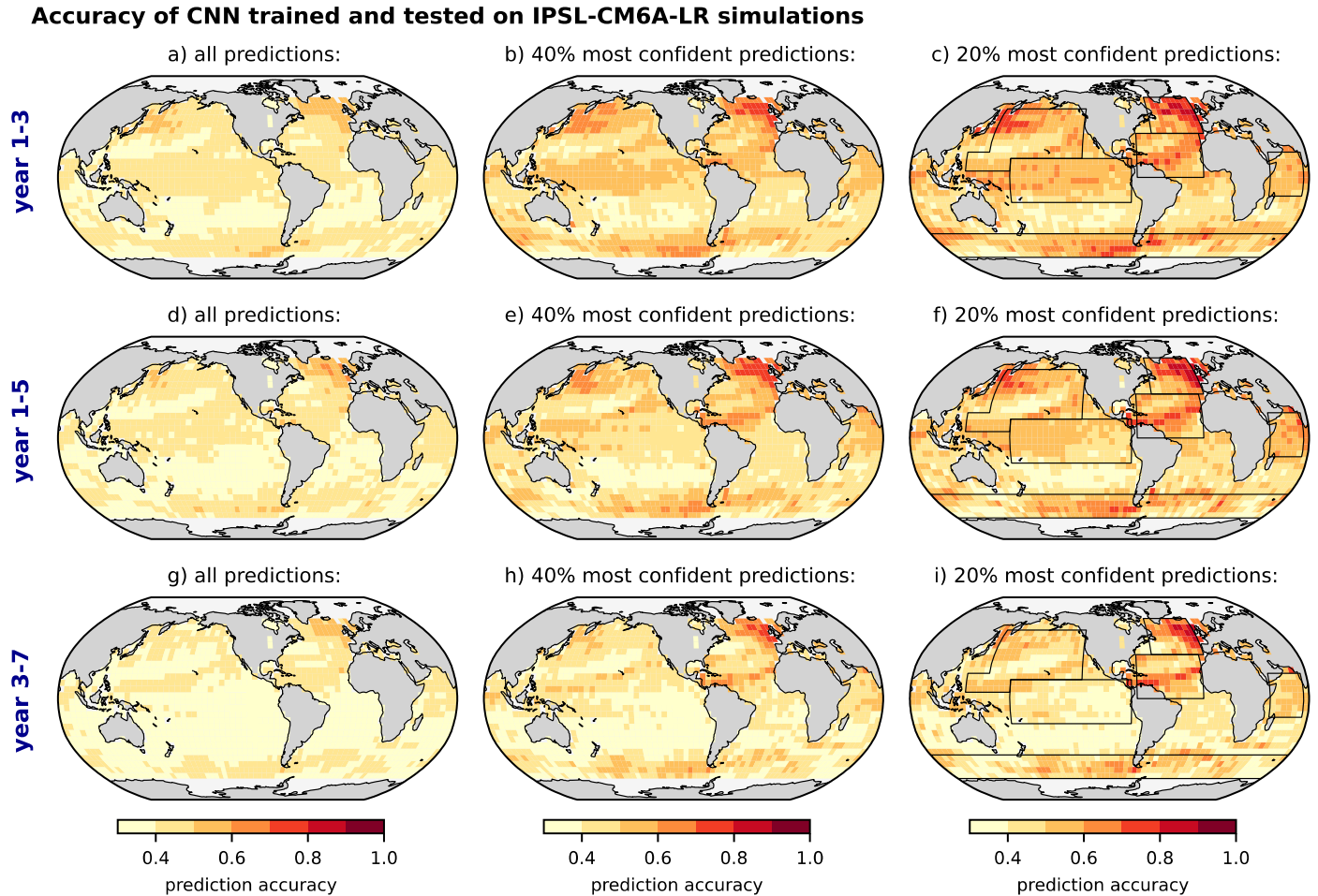
162 *2.4 Evaluating neural network performance on historical observations*

163 We use the NOAA Extended Reconstructed SST Version 5 (ERSSTv5) dataset (Huang et
164 al., 2017) to evaluate how well the trained CNNs can predict historical internal SST variability.
165 The ERSSTv5 dataset includes global coverage at $2^\circ \times 2^\circ$ resolution from 1854 to present. We
166 analyze monthly SST averages from January 1854 through October 2022. We perform similar
167 preprocessing steps as for the GCM simulations. We regrid to the same $5^\circ \times 5^\circ$ grid and calculate
168 12-, 36-, and 60-month moving averages. Then, instead of subtracting the GCM ensemble mean,
169 we subtract the third-order polynomial trend from each grid cell to remove any long-term
170 forcing. We then calculate grid-cell means, standard deviations, and tercile thresholds.

171 In analyzing CNN predictions on the ERSSTv5 data, we focus specifically on windows
172 of opportunity by looking at the accuracy of the top 20% most confident predictions. We also
173 calculate the accuracy of persistence predictions within the ERSSTv5 data as a baseline
174 comparison.

175 **3 Results and Discussion**

176 The CNN accuracy results are shown for one model, *IPSL-CM6-LR*, in Figure 2, with the
 177 remaining models shown in Fig. S2-S9 (*Supporting Information*). Because we have removed the
 178 forced response from the GCM simulations, these maps show the accuracy of predicting internal
 179 SST variability.



180 **Figure 2.** Accuracy of 1-5 year SST predictions using the CNNs trained and tested on *IPSL-*
 181 *CM6A-LR* simulations. **a)** accuracy calculated across all predictions in the test set. **b)** accuracy
 182 calculated for the 40% most confident predictions in the test set (see Methods). **c)** same as b) but
 183 for the 20% most confident predictions. Black boxes indicate regions shown in Fig 4. Other
 184 GCMs are shown in *Supporting Information*, Figs S2-S9.

185 Overall, we find that the prediction accuracy is higher for years 1-3, decreases for years
 186 1-5, and is lowest for years 3-7. This pattern of higher prediction accuracy at shorter lead times is
 187 true across all nine GCMs. When accuracy is calculated across all test samples (e.g. left column
 188 of Fig. 2), the CNNs perform slightly better than the persistence model benchmark (*Supporting*
 189 *Information*, Fig. S10-11). However, we find that the CNNs can make much more skillful
 190 predictions during windows of opportunity, shown in the middle and right columns of Fig. 2. In
 191 some regions, prediction accuracy can approach 80% or higher for these more confident

192 predictions (e.g. Fig. 2c, f). We find that the CNNs are able to identify windows of opportunity
193 with higher prediction accuracy in all of the GCMs analyzed.

194 Regions where future SSTs are predicted most skillfully include the North Pacific,
195 Tropical Pacific, North Atlantic, Tropical Atlantic and the Southern Ocean (defined here to refer
196 to ocean regions between 45-65S). While many of these regions are similar across the different
197 GCMs, there are also clear inter-model differences. For example, CNNs trained and tested on
198 *CNRM-CM6-1* detect especially strong predictability in the North Atlantic (Fig S3). This is likely
199 due to the stronger persistence of SSTs in North Atlantic in this GCM (*Supporting Information*,
200 Fig. S10). The CNNs trained on *CanESM5* or *NorCPM1* have much higher accuracy in
201 predicting SST anomalies in the Southern Ocean compared to other regions. As a third example,
202 the CNNs trained on *GISS-E2-1-G*, *MIROC-ES2L* and *MIROC6* all show strong 1-3 year SST
203 predictability across the tropics, including parts of the Indian Ocean.

204 Within each ocean basin, the spatial pattern of predictability varies depending on the
205 GCM. For example, within the North Atlantic, many of the GCMs have the highest predictability
206 in the subpolar North Atlantic (e.g. *ACCESS-ESM1*, *NorCPM1*). For some GCMs, though, the
207 region of high predictability extends to include a band of high predictability in the subtropical
208 North Atlantic (e.g. *CNRM-CM6-1*, *IPSL-CM6A-LR*). Different GCMs also have different spatial
209 patterns of predictability in the North Pacific. Many GCMs show highest predictability in the
210 subpolar (and especially the western subpolar) North Pacific region. Some models, such as
211 *MIROC-ES2L* and *MIROC6*, show higher predictability in the central North Pacific. In the
212 Southern Ocean, the most predictable region depends on both the GCM and the lead time. Many
213 of the GCMs show high predictability across most of the Southern Ocean for year 1-3
214 predictions. For year 3-7 predictions, the region of high predictability generally narrows to
215 regions of the South Pacific and South Atlantic, especially just west and east of South America
216 (between around 160W to 0W).

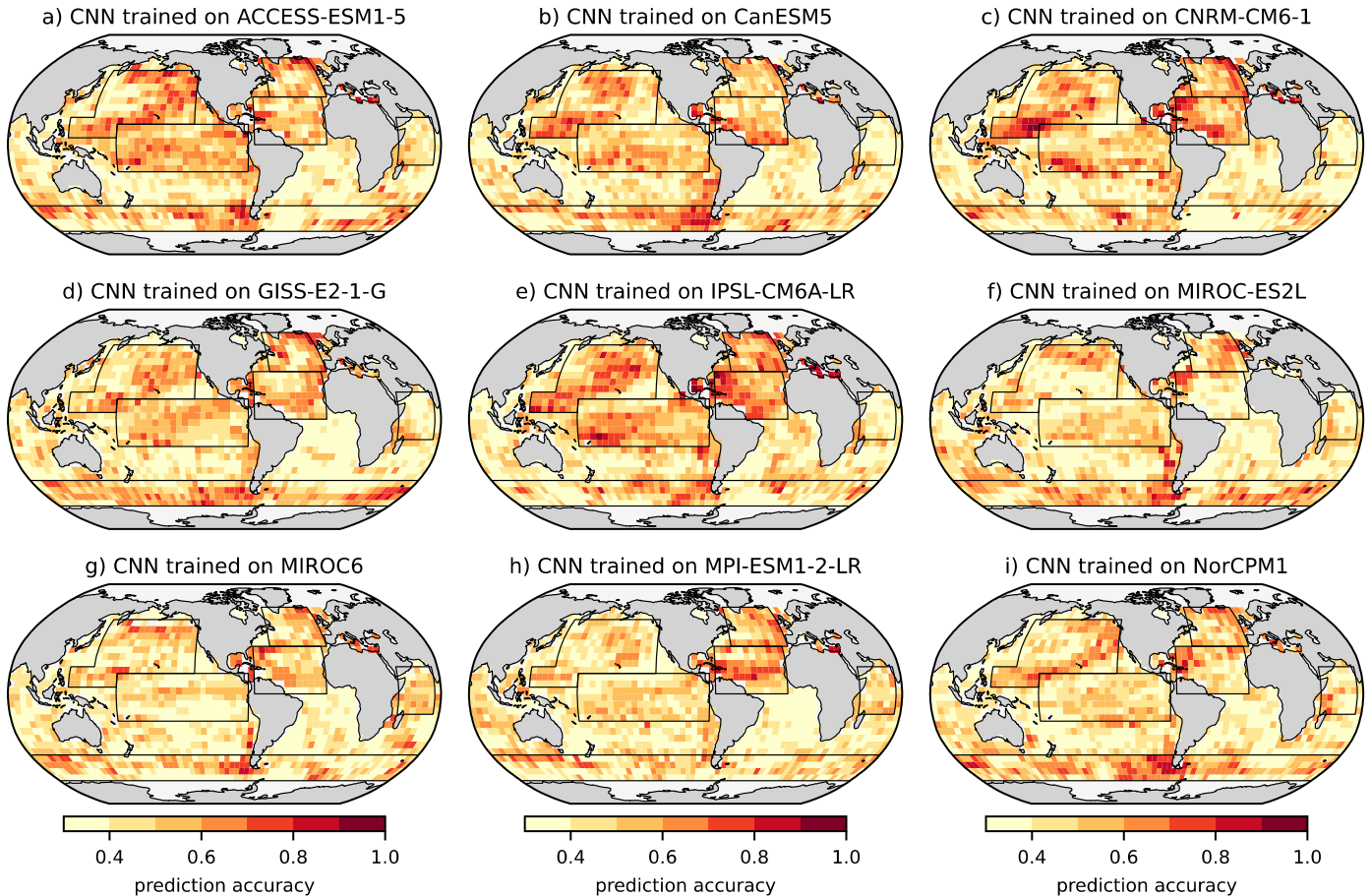
217 After training CNNs on each GCM, we look at how well the CNNs perform when tested
218 on ERSSTv5 observations. These results are shown in Figure 3 for the year 1-5 lead time. Year
219 1-3 and year 3-7 results are shown in *Supporting Information*, Fig. S12-13. We find that the
220 CNNs are able to make skillful predictions using the ERSSTv5 observations, and that the CNN
221 predictions outperform the historical persistence model (*Supporting Information*, Fig. S14).

222 The regions with the most accurate predictions in ERSSTv5 are generally the same
223 regions that were most predictable in the GCMs, namely the North Pacific, Tropical Pacific,
224 North Atlantic, Tropical Atlantic, and Southern Ocean. However, there are also differences in the
225 spatial pattern of predictability between ERSSTv5 and the GCMs. As an example, in the North
226 Pacific, the regions of highest predictability in ERSSTv5 appear similar to the PDO horseshoe
227 pattern in the central/eastern North Pacific (e.g. Fig. 3a-e, i). In contrast, when the CNNs are
228 evaluated on the original GCM test simulations (Fig. 2 and *Supporting Information*, Fig. 2-9),
229 most of the GCMs lack the PDO horseshoe pattern and show the highest predictability in the
230 western subpolar North Pacific. There are also some small regions of predictability in the
231 ERSSTv5 observations that did not appear at all in the GCMs, such as along the coast of Chile.

232 As in the GCM test data, the CNN skill at predicting the ERSSTv5 observations
233 generally decreases at the 3-7 year lead time (Fig. S13). One exception is in the North Pacific for
234 CNNs that were trained on *ACCESS-ESM1-5*, *CNRM-CM6-1*, or *IPSL-CM6A-LR*. We find that
235 these CNNs still make relatively skillful predictions in the North Pacific at 3-7 year lead times

Windows of Opportunity tested on ERSSTv5 observations

Accuracy of 20% most confident predictions of **year 1-5** sea surface temperature anomaly



236 **Figure 3.** Accuracy of 1-5 year SST predictions for *windows of opportunity* (i.e. 20% most
237 most confident predictions) within the ERSSTv5 data. Panels show results for CNNs trained on
238 different GCMs. Other lead times are shown in *Supporting Information*, Fig. S12-13.

239

240 when evaluated on the ERSSTv5 observations. In fact, the CNNs trained on *ACCESS-ESM1-5*
241 and *IPSL-CM6A-LR* predict the ERSSTv5 observations in the North Pacific better than they
242 predict their respective GCM testing data at the 3-7 year lead time (Fig. 4f).

243 Figure 4 summarizes the CNN performance on the GCM testing data versus the
244 ERSSTv5 observations at the global scale (Fig. 4a-c) and for the six regions with the most
245 skillful predictions: North Pacific, Tropical Pacific, Southern Ocean, North Atlantic, Tropical
246 Atlantic, and West Indian Ocean. There are a few interesting patterns that emerge. We find that
247 higher predictability in a GCM does not necessarily lead to higher predictability in the ERSSTv5
248 observations. For example, in the North Pacific for years 1-3 and in the Tropical Pacific for years
249 1-3 and 1-5, the GCMs that correspond to the highest prediction accuracy have lower accuracy
250 when the CNNs are tested on ERSSTv5 (shown by negative correlations in Fig. 4). However, in
251 other locations, such as the Tropical Atlantic for years 1-5 and years 3-7, higher predictability in
252 the GCM does correspond to higher predictability in ERSSTv5. For the most part, prediction

Prediction accuracy in ERSSTv5 dataset vs. GCM simulations

Accuracy of 20% most confident predictions of sea surface temperature

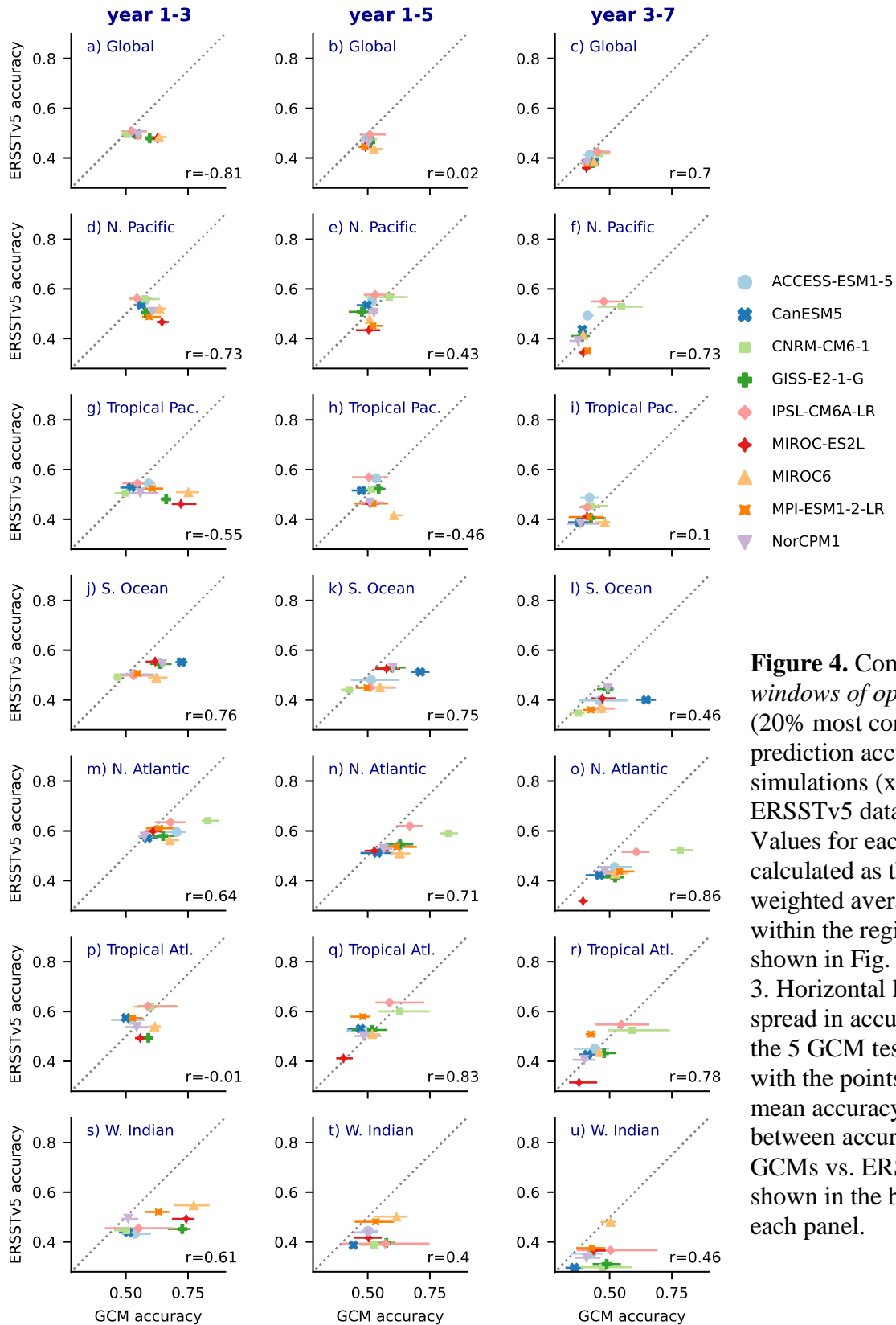


Figure 4. Comparison of *windows of opportunity* (20% most confident) prediction accuracy in GCM simulations (x-axis) vs. the ERSSTv5 data (y-axis). Values for each region are calculated as the area-weighted average accuracy within the region boundaries shown in Fig. 2c,f,i and Fig. 3. Horizontal lines show spread in accuracy across the 5 GCM test simulations, with the points showing the mean accuracy. Correlation between accuracy in the GCMs vs. ERSSTv5 is shown in the bottom right of each panel.

254 accuracy is higher in the original GCM test data than in the ERSSTv5 observations (shown by
255 most points falling below the one-to-one lines). However, in addition to the example given above
256 for the North Pacific, some CNNs can make more skillful predictions in the Tropical Pacific and
257 Tropical Atlantic in ERSSTv5 observations than in the original GCM test data (Fig. 4h, i, p-r).

258 The spread in prediction accuracy across the five ensemble members in each GCM test
259 set is shown by horizontal bars in Fig. 4. In general, the differences in predictability between
260 different GCMs are larger than the differences in predictability between individual simulations.
261 However, we do find that there can be substantial spread in prediction accuracy depending on
262 both the region and the GCM. The West Indian Ocean and Tropical Atlantic have the highest
263 spread in predictability across different simulations (although not in all GCMs). Overall, this
264 indicates that a ~150 year record (the length of our training and testing simulations) may not be
265 sufficient to characterize multiyear predictability at a given location, which should be taken into
266 account when comparing predictability across individual simulations or in the historical record.

267 Overall, many of these results are consistent with prior studies on multidecadal climate
268 prediction. One difference is that we measure prediction skill with classification accuracy and
269 using the window of opportunity framework rather than metrics like the anomaly correlation
270 coefficients. Further, many prior studies on multiyear prediction, including those that use
271 initialized hindcast experiments, evaluate skill in predicting the combined forced response and
272 internal variability. Still, the regions that we find have the most predictability across the GCMs
273 and ERSSTv5 observations include many regions that have been identified in prior work, such as
274 the North Atlantic (Borchert et al., 2021; Yeager et al., 2018; Yeager & Robson, 2017), Southern
275 Ocean (Zhang et al., 2023), and North Pacific (Choi & Son, 2022; Gordon et al., 2021; Qin et al.,
276 2022).

277 Our results also emphasize the importance of considering prediction uncertainty or
278 confidence using the window of opportunity framework. We find many windows of opportunity
279 for multiyear SST predictability, including for most regions, across all GCMs studied, and at all
280 three lead times studied. These findings are aligned with other recent work demonstrating the
281 occurrence of windows of opportunity within the climate system across multiple timescales
282 (Gordon & Barnes, 2022; Mayer & Barnes, 2021).

283 One recurring question within multidecadal prediction is the occurrence of the signal-to-
284 noise paradox, in which a climate model ensemble predicts observed variability better than it
285 predicts individual ensemble members (Eade et al., 2014; Scaife & Smith, 2018). Here, we also
286 find examples where the patterns learned from GCMs lead to more predictable behaviour in the
287 observations compared to the climate models. While we do not attribute our results to the signal-
288 to-noise paradox, it highlights additional differences in predictability between climate models
289 and observations that could be studied in future work.

290 **4 Conclusions**

291 We show that machine learning, specifically convolutional neural networks, can learn
292 patterns of global, multiyear SST predictability from existing, uninitialized climate model
293 simulations. Because our approach does not require new GCM simulations, we can efficiently
294 analyze and compare predictability across many different GCMs. We find that the regions with
295 the highest predictability on interannual and decadal lead times include the North Pacific, North
296 Atlantic, Tropical Pacific, Tropical Atlantic and the Southern Ocean. However, when comparing

297 predictability across nine GCMs, we find notable differences in the spatial patterns and
298 magnitude of SST prediction skill. The patterns learned by the CNNs also lead to skillful
299 predictions when tested on historical SST observations, but the amount of prediction skill in each
300 region varies based on the GCM used for training. We also find different spatial patterns of SST
301 predictability in the ERSSTv5 observations compared to the GCMs, although the most
302 predictable regions are generally similar.

303 These results could lead to multiple future research directions. It is beyond the scope of
304 the current study to explore why differences in SST predictability exist across GCMs and the
305 observations. However, recent related work has shown that “explainable ML” methods can be
306 used to understand why CNNs make certain predictions (Davenport & Diffenbaugh, 2021;
307 Gordon et al., 2021; Labe & Barnes, 2021; Toms et al., 2020). These same methods could be
308 applied to the CNNs used here to understand the sources of SST predictability and how they
309 differ across GCMs and observations, providing insight into both the mechanisms involved in
310 multiyear variability and into GCM biases in how these mechanisms are represented. Further,
311 while the focus of this study was to explore differences in predictability across GCMs, future
312 efforts could focus on training CNNs to produce the best predictions in the observed climate.
313 This might be accomplished by selecting certain GCMs to use as training data for different
314 regions, or using a combination of GCM and observational data for training through approaches
315 like transfer learning (e.g. Ham et al., 2019). Overall, this research supports a growing body of
316 literature that shows ML is a valuable tool for advancing the field of skillful multiyear climate
317 prediction.

318

319 **Acknowledgments**

320 This work was funded, in part, by grant AGS-2210068 from the National Science
321 Foundation and with special thanks to David Wallerstein.

322

323 **Data Availability**

324 We use historical simulations from the CMIP6 archive available through the Earth
325 System Grid (<https://esgf-node.llnl.gov/projects/cmip6/>). We use historical sea surface
326 temperature data from the ERSSTv5 dataset available from the National Oceanic and
327 Atmospheric Administration (<https://psl.noaa.gov/data/gridded/data.noaa.ersst.v5.html>).

328

329 **Code Availability**

330 The analysis code used to train the convolutional neural networks and generate figures in
331 the paper will be made available on github and archived using Zenodo (DOI will be created and
332 provided here before publication).

333

334

335 **References**

- 336 Bethke, I., Wang, Y., Counillon, F., Keenlyside, N., Kimmritz, M., Fransner, F., et al. (2021).
337 NorCPM1 and its contribution to CMIP6 DCP. *Geoscientific Model Development*,
338 *14*(11), 7073–7116. <https://doi.org/10.5194/gmd-14-7073-2021>
- 339 Borchert, L. F., Menary, M. B., Swingedouw, D., Sgubin, G., Hermanson, L., & Mignot, J.
340 (2021). Improved Decadal Predictions of North Atlantic Subpolar Gyre SST in CMIP6.
341 *Geophysical Research Letters*, *48*(3), e2020GL091307.
342 <https://doi.org/10.1029/2020GL091307>
- 343 Boucher, O., Servonnat, J., Albright, A. L., Aumont, O., Balkanski, Y., Bastrikov, V., et al.
344 (2020). Presentation and Evaluation of the IPSL-CM6A-LR Climate Model. *Journal of*
345 *Advances in Modeling Earth Systems*, *12*(7). <https://doi.org/10.1029/2019MS002010>
- 346 Cassou, C., Kushnir, Y., Hawkins, E., Pirani, A., Kucharski, F., Kang, I.-S., & Caltabiano, N.
347 (2018). Decadal Climate Variability and Predictability: Challenges and Opportunities.
348 *Bulletin of the American Meteorological Society*, *99*(3), 479–490.
349 <https://doi.org/10.1175/BAMS-D-16-0286.1>
- 350 Choi, J., & Son, S.-W. (2022). Seasonal-to-decadal prediction of El Niño–Southern Oscillation
351 and Pacific Decadal Oscillation. *Npj Climate and Atmospheric Science*, *5*(1), 29.
352 <https://doi.org/10.1038/s41612-022-00251-9>
- 353 Davenport, F. V., & Diffenbaugh, N. S. (2021). Using Machine Learning to Analyze Physical
354 Causes of Climate Change: A Case Study of U.S. Midwest Extreme Precipitation.
355 *Geophysical Research Letters*, *48*(15), e2021GL093787.
356 <https://doi.org/10.1029/2021GL093787>

357 Delgado-Torres, C., Donat, M. G., Gonzalez-Reviriego, N., Caron, L.-P., Athanasiadis, P. J.,
358 Bretonnière, P.-A., et al. (2022). Multi-Model Forecast Quality Assessment of CMIP6
359 Decadal Predictions. *JOURNAL OF CLIMATE*, 35.

360 Eade, R., Smith, D., Scaife, A., Wallace, E., Dunstone, N., Hermanson, L., & Robinson, N.
361 (2014). Do seasonal-to-decadal climate predictions underestimate the predictability of the
362 real world? *Geophysical Research Letters*, 41(15), 5620–5628.
363 <https://doi.org/10.1002/2014GL061146>

364 Enfield, D. B., Mestas-Nuñez, A. M., & Trimble, P. J. (2001). The Atlantic Multidecadal
365 Oscillation and its relation to rainfall and river flows in the continental U.S. *Geophysical*
366 *Research Letters*, 28(10), 2077–2080. <https://doi.org/10.1029/2000GL012745>

367 Eyring, V., Bony, S., Meehl, G. A., Senior, C. A., Stevens, B., Stouffer, R. J., & Taylor, K. E.
368 (2016). Overview of the Coupled Model Intercomparison Project Phase 6 (CMIP6)
369 experimental design and organization. *Geoscientific Model Development*, 9(5), 1937–
370 1958. <https://doi.org/10.5194/gmd-9-1937-2016>

371 Findell, K. L., Sutton, R., Caltabiano, N., Brookshaw, A., Heimbach, P., Kimoto, M., et al.
372 (2023). Explaining and Predicting Earth System Change: A World Climate Research
373 Programme Call to Action. *Bulletin of the American Meteorological Society*, 104(1),
374 E325–E339. <https://doi.org/10.1175/BAMS-D-21-0280.1>

375 Gordon, E. M., & Barnes, E. A. (2022). Incorporating Uncertainty into a Regression Neural
376 Network Enables Identification of Decadal State-Dependent Predictability. *Geophysical*
377 *Research Letters*, 49(e2022GL098635). <https://doi.org/10.1029/2022GL098635>

378 Gordon, E. M., Barnes, E. A., & Hurrell, J. W. (2021). Oceanic Harbingers of Pacific Decadal
379 Oscillation Predictability in CESM2 Detected by Neural Networks. *Geophysical*
380 *Research Letters*, 48, e2021GL095392. <https://doi.org/10.1029/2021GL095392>

381 Gordon, E. M., Barnes, E. A., & Davenport, F. V. (2023). Separating internal and forced
382 contributions to near term SST predictability in the CESM2-LE. *Environmental Research*
383 *Letters*, 18(10), 104047. <https://doi.org/10.1088/1748-9326/acfdbbc>

384 Hajima, T., Watanabe, M., Yamamoto, A., Tatebe, H., Noguchi, M. A., Abe, M., et al. (2020).
385 Development of the MIROC-ES2L Earth system model and the evaluation of
386 biogeochemical processes and feedbacks. *Geoscientific Model Development*, 13(5),
387 2197–2244. <https://doi.org/10.5194/gmd-13-2197-2020>

388 Ham, Y. G., Kim, J. H., & Luo, J. J. (2019). Deep learning for multi-year ENSO forecasts.
389 *Nature*, 573(7775), 568–572. <https://doi.org/10.1038/s41586-019-1559-7>

390 Huang, B., Thorne, P. W., Banzon, V. F., Boyer, T., Chepurin, G., Lawrimore, J. H., et al.
391 (2017). Extended Reconstructed Sea Surface Temperature, Version 5 (ERSSTv5):
392 Upgrades, Validations, and Intercomparisons. *Journal of Climate*, 30(20), 8179–8205.
393 <https://doi.org/10.1175/JCLI-D-16-0836.1>

394 Kelley, M., Schmidt, G. A., Nazarenko, L. S., Bauer, S. E., Ruedy, R., Russell, G. L., et al.
395 (2020). GISS-E2.1: Configurations and Climatology. *Journal of Advances in Modeling*
396 *Earth Systems*, 12(8). <https://doi.org/10.1029/2019MS002025>

397 Kushnir, Y., Scaife, A. A., Arritt, R., Balsamo, G., Boer, G., Doblas-Reyes, F., et al. (2019).
398 Towards operational predictions of the near-term climate. *Nature Climate Change*, 9(2),
399 94–101. <https://doi.org/10.1038/s41558-018-0359-7>

400 Labe, Z. M., & Barnes, E. A. (2021). Detecting Climate Signals Using Explainable AI With
401 Single-Forcing Large Ensembles. *Journal of Advances in Modeling Earth Systems*, 13(6),
402 e2021MS002464. <https://doi.org/10.1029/2021MS002464>

403 Labe, Z. M., & Barnes, E. A. (2022). Predicting Slowdowns in Decadal Climate Warming
404 Trends With Explainable Neural Networks. *Geophysical Research Letters*, 49(9).
405 <https://doi.org/10.1029/2022GL098173>

406 Martin, E. R., & Thorncroft, C. (2014). Sahel rainfall in multimodel CMIP5 decadal hindcasts.
407 *Geophysical Research Letters*, 41(6), 2169–2175. <https://doi.org/10.1002/2014GL059338>

408 Mauritsen, T., Bader, J., Becker, T., Behrens, J., Bittner, M., Brokopf, R., et al. (2019).
409 Developments in the MPI-M Earth System Model version 1.2 (MPI-ESM1.2) and Its
410 Response to Increasing CO₂. *Journal of Advances in Modeling Earth Systems*, 11(4),
411 998–1038. <https://doi.org/10.1029/2018MS001400>

412 Mayer, K. J., & Barnes, E. A. (2021). Subseasonal Forecasts of Opportunity Identified by an
413 Explainable Neural Network. *Geophysical Research Letters*, 48(10), e2020GL092092.
414 <https://doi.org/10.1029/2020GL092092>

415 Meehl, G. A., Goddard, L., Murphy, J., Stouffer, R. J., Boer, G., Danabasoglu, G., et al. (2009).
416 Decadal Prediction: Can It Be Skillful? *Bulletin of the American Meteorological Society*,
417 90(10), 1467–1486. <https://doi.org/10.1175/2009BAMS2778.1>

418 Meehl, G. A., Richter, J. H., Teng, H., Capotondi, A., Cobb, K., Doblas-Reyes, F., et al. (2021).
419 Initialized Earth System prediction from subseasonal to decadal timescales. *Nature*
420 *Reviews Earth & Environment*, 2(5), 340–357. [https://doi.org/10.1038/s43017-021-](https://doi.org/10.1038/s43017-021-00155-x)
421 00155-x

422 Meehl, G. A., Teng, H., Smith, D., Yeager, S., Merryfield, W., Doblas-Reyes, F., & Glanville, A.
423 A. (2022). The effects of bias, drift, and trends in calculating anomalies for evaluating
424 skill of seasonal-to-decadal initialized climate predictions. *Climate Dynamics*, 59(11–12),
425 3373–3389. <https://doi.org/10.1007/s00382-022-06272-7>

426 Qin, M., Du, Z., Hu, L., Cao, W., Fu, Z., Qin, L., et al. (2022). Deep Learning for Multi-
427 Timescales Pacific Decadal Oscillation Forecasting. *Geophysical Research Letters*,
428 49(6). <https://doi.org/10.1029/2021GL096479>

429 Risbey, J. S., Squire, D. T., Black, A. S., DelSole, T., Lepore, C., Matear, R. J., et al. (2021).
430 Standard assessments of climate forecast skill can be misleading. *Nature*
431 *Communications*, 12(1), 4346. <https://doi.org/10.1038/s41467-021-23771-z>

432 Scaife, A. A., & Smith, D. (2018). A signal-to-noise paradox in climate science. *Npj Climate and*
433 *Atmospheric Science*, 1(1), 28. <https://doi.org/10.1038/s41612-018-0038-4>

434 Simpson, I. R., Yeager, S. G., McKinnon, K. A., & Deser, C. (2019). Decadal predictability of
435 late winter precipitation in western Europe through an ocean–jet stream connection.
436 *Nature Geoscience*, 12(8), 613–619. <https://doi.org/10.1038/s41561-019-0391-x>

437 Smith, D. M., Eade, R., Dunstone, N. J., Fereday, D., Murphy, J. M., Pohlmann, H., & Scaife, A.
438 A. (2010). Skilful multi-year predictions of Atlantic hurricane frequency. *Nature*
439 *Geoscience*, 3(12), 846–849. <https://doi.org/10.1038/ngeo1004>

440 Sutton, R. T., & Hodson, D. L. R. (2005). Atlantic Ocean Forcing of North American and
441 European Summer Climate. *Science*, 309(5731), 115–118.
442 <https://doi.org/10.1126/science.1109496>

443 Swart, N. C., Cole, J. N. S., Kharin, V. V., Lazare, M., Scinocca, J. F., Gillett, N. P., et al.
444 (2019). The Canadian Earth System Model version 5 (CanESM5.0.3). *Geoscientific*
445 *Model Development*, 12(11), 4823–4873. <https://doi.org/10.5194/gmd-12-4823-2019>

446 Tatebe, H., Ogura, T., Nitta, T., Komuro, Y., Ogochi, K., Takemura, T., et al. (2019).
447 Description and basic evaluation of simulated mean state, internal variability, and climate
448 sensitivity in MIROC6. *Geoscientific Model Development*, 12(7), 2727–2765.
449 <https://doi.org/10.5194/gmd-12-2727-2019>

450 Toms, B. A., Barnes, E. A., & Ebert-Uphoff, I. (2020). Physically Interpretable Neural Networks
451 for the Geosciences: Applications to Earth System Variability. *Journal of Advances in*
452 *Modeling Earth Systems*, 12(9), e2019MS002002.
453 <https://doi.org/10.1029/2019MS002002>

454 Toms, B. A., Barnes, E. A., & Hurrell, J. W. (2021). Assessing Decadal Predictability in an
455 Earth-System Model Using Explainable Neural Networks. *Geophysical Research Letters*,
456 48(12), e2021GL093842. <https://doi.org/10.1029/2021GL093842>

457 Van Oldenborgh, G. J., Doblas-Reyes, F. J., Wouters, B., & Hazeleger, W. (2012). Decadal
458 prediction skill in a multi-model ensemble. *Climate Dynamics*, 38(7–8), 1263–1280.
459 <https://doi.org/10.1007/s00382-012-1313-4>

460 Voltaire, A., Saint-Martin, D., Sénési, S., Decharme, B., Alias, A., Chevallier, M., et al. (2019).
461 Evaluation of CMIP6 DECK Experiments With CNRM-CM6-1. *Journal of Advances in*
462 *Modeling Earth Systems*, 11(7), 2177–2213. <https://doi.org/10.1029/2019MS001683>

463 Yeager, S. G., & Robson, J. I. (2017). Recent Progress in Understanding and Predicting Atlantic
464 Decadal Climate Variability. *Current Climate Change Reports*, 3(2), 112–127.
465 <https://doi.org/10.1007/s40641-017-0064-z>

466 Yeager, S. G., Danabasoglu, G., Rosenbloom, N. A., Strand, W., Bates, S. C., Meehl, G. A., et
467 al. (2018). Predicting Near-Term Changes in the Earth System: A Large Ensemble of
468 Initialized Decadal Prediction Simulations Using the Community Earth System Model.
469 *Bulletin of the American Meteorological Society*, 99(9), 1867–1886.
470 <https://doi.org/10.1175/BAMS-D-17-0098.1>

471 Zhang, L., Delworth, T. L., Yang, X., Morioka, Y., Zeng, F., & Lu, F. (2023). Skillful decadal
472 prediction skill over the Southern Ocean based on GFDL SPEAR Model-Analogs.
473 *Environmental Research Communications*, 5(2), 021002. [https://doi.org/10.1088/2515-](https://doi.org/10.1088/2515-7620/acb90e)
474 [7620/acb90e](https://doi.org/10.1088/2515-7620/acb90e)

475 Ziehn, T., Chamberlain, M. A., Law, R. M., Lenton, A., Bodman, R. W., Dix, M., et al. (2020).
476 The Australian Earth System Model: ACCESS-ESM1.5. *Journal of Southern Hemisphere*
477 *Earth Systems Science*, 70(1), 193. <https://doi.org/10.1071/ES19035>
478
479